Iranian Journal of Science and Technology, Transactions of Civil Engineering (2024) 48:97–115
https://doi.org/10.1007/s40996-023-01168-w

RESEARCH PAPER

The Effect of RHA and GBFS on the Mechanical and Physical Properties of Cementitious Composites with High Early Age Compressive and Flexural Strength: Bayesian Algorithm for the Design

Oguzhan Yavuz Bayraktar[1] · **Fadel Mohamed Ali Fello**[2]

Received: 15 March 2023 / Accepted: 3 June 2023 / Published online: 28 June 2023

Abstract

In recent years, cementitious composites with a compressive strength of more than 100 MPa have become popular for tall earthquake-resistant buildings. However, in these composites, attention is paid to sustainability criteria along with strength. In this study, physical, mechanical, and microstructural properties of cementitious composites with high early-age strength were investigated by using industrial wastes such as RHA (rice husk ash) and GBFS (ground blast furnace slag). In cementitious composites, the cement dosage was chosen as 1000 kg and the w/c (water/cement) or w/b (water/binder) ratio was 0.22. RHA was used instead of cement at the rate of 5 and 10%, and GBFS at the rate of 5, 10, and 15%. Cementitious composites were subjected to three different cures: normal water (WC), hot water (HWC), and steam (SC). As the RHA content increased, the flow diameter of the mixtures decreased. GBFS relatively improved the workability of cementitious composites. While the porosity of WC applied mixtures varies between 2.7 and 4.3%, the porosity of HWC or SC applied mixtures decreases up to 1.3%. The water absorption of all cementitious composites is less than 2%. The 3-day compressive strengths of the mixtures are between 53.4 and 90.6 MPa, and the 90-day compressive strengths are between 100.2 and 123.3 MPa. In addition, the 3-day flexural strength of the mixtures exceeds 7 MPa. On the 90th day, cementitious composites with a flexural strength of approximately 18 MPa were produced. As the RHA content increased, it decreased the 3-day flexural and compressive strengths but improved the mechanical properties on the 90th day. Dense needle-like CSH gels were observed in SEM examinations. With the developed ANN model, it has been determined that the material quantities (RHA and GBFS content) and curing conditions will be predicted with high accuracy for optimum compressive strength. As a result, it has been determined that a compressive strength higher than 120 MPa and a flexural strength higher than 15 MPa will be obtained by saving 25% cement.

Keywords Bayesian algorithm · Ground blast furnace slag · Recycling · Rice husk ash · Sustainability

1 Introduction

Global climate change caused by greenhouse gas emissions is accelerating day by day. Today, global efforts to reduce the effects of greenhouse gas emissions and policies promoting carbon neutrality are followed (Han et al. 2022). Research is being carried out to reduce CO_2 emissions in many areas around the World (Kaplan et al. 2018; Sevik et al. 2018; Bayraktar 2019, 2021; Bayraktar et al. 2019; Turkyilmaz et al. 2020; Elsunousi et al. 2021; Varol et al. 2021, 2022). Cement production is one of the sectors with the highest CO_2 emissions in the world. During the production of ordinary Portland cement, approximately 10% of CO_2 is emitted to the atmosphere (Chang et al. 2019). CO_2 is emitted during the sintering and grinding of clinker and the shipment of cement. Especially the CO_2 emission that is released during the sintering of the clinker constitutes 80% of the total CO_2 emission (Maddalena et al. 2018; Lippiatt et al. 2020). In the sintering process, the CO_2 in the limestone is separated and its interaction with the clay is provided. For this interaction, the furnace temperature should be approximately 1450 °C. Large amounts of fossil fuels are used to achieve

✉ Oguzhan Yavuz Bayraktar
obayraktar@kastamonu.edu.tr

[1] Civil Engineering Department, Kastamonu University, 37150 Kastamonu, Turkey

[2] Department of Materials Science and Engineering, Kastamonu University, 37150 Kastamonu, Turkey

this target temperature. Using fossil fuels in cement production is responsible for 30% of CO_2 emissions. Removing CO_2 from the limestone is responsible for 50% of the CO_2 emissions. Therefore, CO_2 is emitted at almost every stage of cement production. Industrial wastes such as fly ash (FA), ground blast furnace slag (GBFS) or rice husk ash (RHA) should be used instead of cement to reduce the CO_2 emission in cement production (Wang and Scrivener 1995; Singh et al. 2015).

GBFS is a waste material from the blast furnace in iron production (Cheah et al. 2022). GBFS is one of the materials preferred to reduce CO_2 emissions in cement and concrete production (Yun et al. 2020). Crossin reported a 47.5% reduction in greenhouse gas emissions when GBFS is used instead of cement in concrete production (Crossin 2015). In GBFS production, 10% less CO_2 is released and 20% less energy is consumed than cement production (Atici and Ersoy 2008). Studies have shown that GBFS reduces early age strength due to its slow hydraulic and pozzolanic properties. However, it has been stated that it improves the mechanical properties at the age of 28 and above (Boubekeur et al. 2019; Lim et al. 2019; Suda and Rao 2020). In addition, it has been proven in many studies that GBFS contributes positively to the durability of concrete (Li et al. 2018; Angulo-Ramirez et al. 2019; Ghorbani et al. 2023). It has also been stated that GBFS greatly reduces the chloride permeability of concrete (Shubbar et al. 2018).

Another industrial waste used in concrete and cement production is RHA. RHA, an agricultural by-product of rice cultivation, is mostly used for fuel (Jittin et al. 2020; Subashi De Silva et al. 2021). A large amount of RHA is released in the agricultural sector, especially in Asian countries. In 2017, world paddy production was approximately 759 million tons. In Asian countries, 689 million tons of RHA (about 91% of the total) were formed. As a result of the burning of rice husk, approximately 20% RHA is obtained (Muntohar 2002). Since RHA contains a high percentage of SiO_2 and glassy phase (amorphous structure), it can be used in cement and concrete production (De Silva and Perera 2018; Moayedi et al. 2019). It has been stated that RHA improves the microstructure, durability, and strength of cementitious systems due to its pozzolanic and filler properties (Kanthe 2021; Nduka et al. 2022; Tayeh et al. 2022; Çelik et al. 2023; Kramer et al. 2023). Jamil et al. obtained compressive strengths in the mortars' range of 10.1–21.5 MPa on the 90th day. They used 20% RHA (Jamil et al. 2016). On the other hand, Miyandehi et al. reported that the compressive strength of the mortars using 30% RHA decreased approximately 30% on the 28th day (Miyandehi et al. 2016). Sensale stated that sulfate damage is reduced when RHA is used in cement-based composites (Rodríguez De Sensale 2010). As a result, it is recommended to use RHA building materials in terms of sustainability (Gupta et al. 2020). It is possible to reduce CO_2 emissions by using RHA and GBFS in many cementitious systems. In addition, such materials reduce the cost of building materials.

RHA and GBFS are frequently used in the high-strength mortar or concretes, ultra-high-performance concrete or mortars. Recently, the production of ultra-high performance concretes with a compressive strength of 200 MPa and above, used in high-rise buildings, has become widespread (Shin et al. 2018). If high-strength cementitious composites are used in structures, the dimensions of the building elements will be reduced. In this way, the dead load of the structures will be reduced. In addition, thanks to the high strength, the composite's elasticity modulus and durability properties will increase. Using high-strength concrete or mortars will not only reduce the building cost but also increase the stability of the structures (Razvi and Saatcioglu 1999). In the last 10 years, much research has been done on high-strength and high-performance mortar or concrete (Jakhrani et al. 2019; Sarıdemir et al. 2020, 2021; Li et al. 2022; Hakeem et al. 2023).

This study investigated the mechanical, physical and microstructural properties of cementitious composites containing RHA and GBFS with high early age compressive and flexural strength. In addition, the effect of different curing conditions (water curing, hot water curing and steam curing) on obtaining a compressive strength of more than 100 MPa was also investigated. ANN model is also proposed to predict high compressive strength with material properties and curing conditions.

2 Experimental Program

2.1 Raw Materials

In this study, CEM I 42.5 R type cement in accordance with EN 197-1 standard was used to make cementitious composites. Ground GBFS has a high glassy phase content and complies with ASTM C989 standard. It is seen in the XRD pattern in Fig. 1 that GBFS is glassy. In GBFS, peaks such as quartz, calcite, gypsum and C_2S were observed. The average particle size of cement and GBFS is 26.6 and 15.9 µm, respectively. The physical and chemical properties of cement, RHA and GBFS are presented in Table 1. The particle size distribution (PSD) of powder materials is shown in Table 1. According to PSD analysis, RHA and GBFS have smaller particle size than OPC. RHA is obtained as a result of burning the husks obtained from the rice factory. A traditional stove was used from the combustion of RHA. RHA was obtained under uncontrolled combustion conditions. The ash formed as a result of the combustion was ground in a ball mill for 2 h. The average grain size of the RHA obtained from milling is 10.7 µm. It was determined in

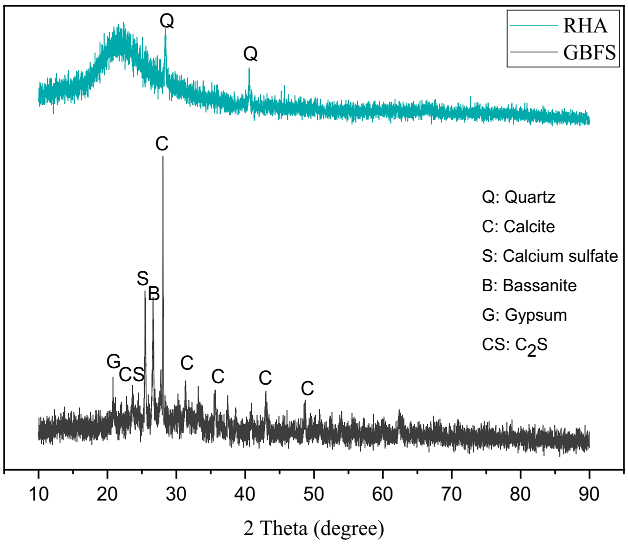

Fig. 1 XRD pattern of GBFS and RHA

the XRD pattern that RHA has glassy phases. Quartz peaks were observed according to the XRD pattern. The physical and chemical properties of RHA are given in Table 2. Table 2 also gives some of the RHA features included in the literature.

This study used silica sand conforming to the ASTM C33 standard. The sieve opening of silica sand is 0–2 mm. Silica sand's specific gravity and water absorptions are 2.66 and 2.1%, respectively. A polycarboxylate-based superplasticizer (SP) was used to improve the workability of cementitious composites. The specific gravity and solids content of the polycarboxylate-based superplasticizer are 1.07 ± 3 and 32%, respectively. Drinkable tap water was used in the preparation and curing of the mixtures.

2.2 Mixing, Casting, and Curing

Cement dosage was chosen as 1000 kg/m^3 in the preparation of the mixtures. Cement dosage was kept high to increase early age strength. The water/cement (w/c) or water/binder (w/b) ratio of all mixtures is 0.22. In addition, the aggregate/binder ratio was chosen as 1 in all mixtures. To ensure adequate workability, 2% of the binder amount of SP was used. GBFS was used instead of cement at the rates of 5, 10, and 15%, and RHA at the rates of 5 and 10%. GBFS and RHA were used by weight instead of cement. In this context, a total of 12 different mixtures were prepared. The amounts of materials used in cementitious composites are given in Table 3.

First, the binding materials (cement + GBFS + RHA) were mixed for 1 min. Afterwards, 2/3 of the water and half of the SP were added to the mixture and mixed for 2 min. After the mixture rested for 1 min, the remaining water and SP were added to the mixture and mixed for 2 more minutes. Finally, silica sand was added to the mixture and mixed for another 5 min. All mixtures obtained have the property of self-compacting.

Three different curing processes were investigated on cementitious composites. These are water cure (WC), hot water cure (HWC) and steam cure (SC). In the WC, the samples were kept in water at a temperature of approximately 24 °C until the day of the experiment. In HWC, the samples were kept in hot water at 60 °C for 24 h. After 24 h, the samples were kept in a curing room (25 °C, 70%

Table 1 Physical and chemical properties of GBFS, RHA, and cement

Oxide (by mass, %)	GBFS	OPC	RHA
SiO_2	14.3	17.8	81.1
Al_2O_3	7.8	5.2	2.2
Fe_2O_3	25.4	3.3	1.4
CaO	31.4	65.5	1.4
MgO	7.2	1.4	2.5
SO_3	0.5	2.6	0.6
K_2O	0.1	0.7	2.8
Na_2O	0.09	0.4	0.3
Specific gravity	2.92	3.14	2.34
SSA*	4760	3370	5970

*Blaine method (cm^2/g)

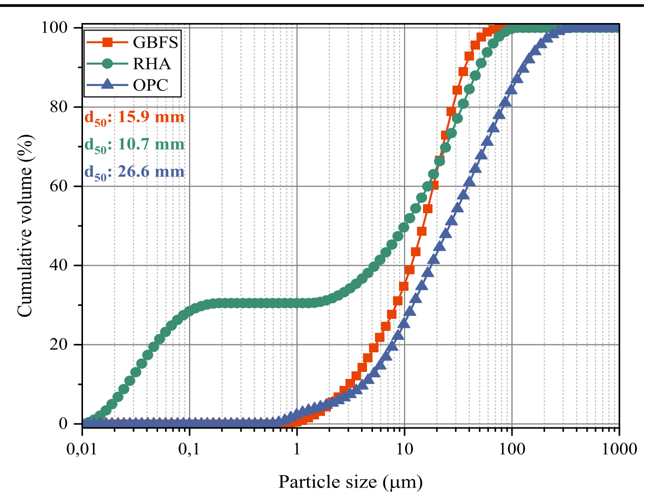

relative humidity) until the test day. Samples were kept in a steam environment at 60 °C for 24 h in SC. After the curing period, the samples were subjected to curing room. As a result of three curing conditions applied to 12 different mixtures, the properties of 36 different cementitious

Table 2 Physical and chemical properties of RHA

Oxide (by mass, %)	This study	Nasiru et al. (2021)	Selvaranjan et al. (2021)	Cordeiro et al. (2009)	Umasabor and Okovido (2018)
SiO_2	86.55	91.90	87.4	82.6	87.22
Al_2O_3	0.55	0.28	1.2	0.4	0.70
Fe_2O_3	0.31	0.19	0.7	0.5	1.68
CaO	0.60	1.15	2.5	0.9	2.12
MgO	0.88	0.71	1.1		1.18
SO_3	0.21	0.22	1.0	0.1	0.05
K_2O	2.28	3.99	1.7	1.8	1.12
Na_2O	1.07	0.04	0.4	0.1	0.20
LOI	9.67	6.7	3.9	11.9	1.06
Specific gravity	2.24		2.34		
SSA (Blaine)	5200				

Table 3 Amounts of materials (kg)

Mix ID	OPC	Water	GBFS	RHA	Silica sand	SP
G0R0	1000	220	0	0	1000	20
G0R5	950	220	0	50	1000	20
G0R10	900	220	0	100	1000	20
G5R0	950	220	50	0	1000	20
G5R5	900	220	50	50	1000	20
G5R10	850	220	50	100	1000	20
G10R0	900	220	100	0	1000	20
G10R5	850	220	100	50	1000	20
G10R10	800	220	100	100	1000	20
G15R0	850	220	150	0	1000	20
G15R5	800	220	150	50	1000	20
G15R10	750	220	150	100	1000	20

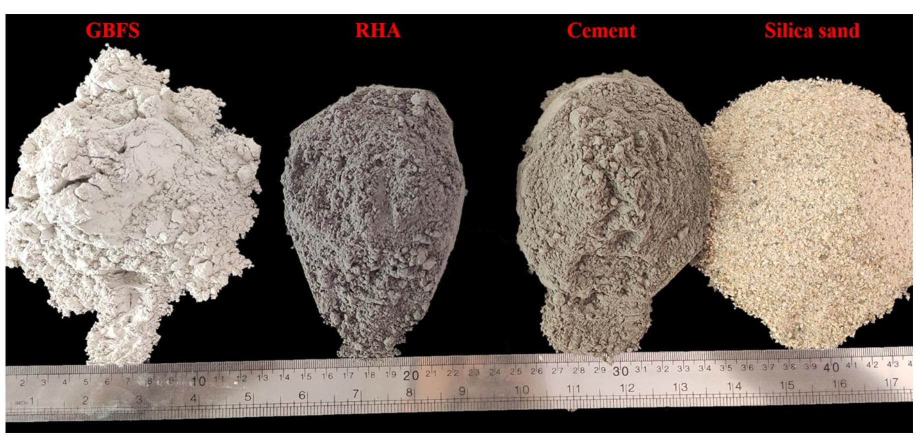

Fig. 2 General view of materials

composites were investigated. Figure 2 presents the general view of the materials used in the experimental study.

2.3 Test Methods

Firstly, the flow diameters of cementitious composites were measured using the ASTM C1437 standard. Flow table apparatus was used for this. The mixtures' apparent porosity, water absorption and unit weight were measured in cube samples with 50 × 50 × 50 mm margins. For this, the ASTM C642 standard and Archimedes method were used. The physical properties of cementitious composites were measured on the 90th day. ASTM C348 and ASTM C 349 standards were used for the flexural and compressive strengths of the mixtures, respectively. Mechanical properties of cementitious composites were measured at 3, 7, 28 and 90 days. 40 × 40 × 160 mm prisms were used to determine the flexural strengths, and samples broken at flexural strength were used for compressive strengths.

Quanta FEG 250 model SEM (scanning electron microscopy) device was used to determine the microstructure of cementitious composites. Microstructure studies were carried out in the MERLAB unit of Kastamonu University. SEM studies were performed at different magnifications.

2.4 Artificial Neural Network (ANN) Modeling

Machine learning applications are used to model and predict real-life problems because they can describe complex relationships between a data set of inputs and outputs without any predetermined equations (Taffese and Sistonen 2017; Lau et al. 2019). This study aims to create a model based on estimating the 28-day compressive strength based on the composition of cementitious composites. In addition to the RHA and GBFS content of cementitious composites, the curing processes that affect the strength were used in the model. An ANN model includes a computational system that mimics the self-learning abilities of neurons in the biological nervous system to map complex interactions between variables. ANN, an important subset of Artificial Intelligence, is used in many fields today (Suleiman and Nehdi 2017). ANN models have been used in many civil engineering problems since the late 1980s (Kaplan et al. 2019; Ganesh and Muthukannan 2021; Sun et al. 2022). ANN consists of three different layers: input, hidden and output (Okwu and Tartibu 2021). In this study, RHA, GBFS content and curing conditions constitute the input layer. The 28-day compressive strength of cementitious composites is the output layer. In the model, this method was used because the Tan-Sigmond function for the neural transmission provides higher computational performance. Bayesian regularization algorithm is used as a precaution to improve ANN generalization and prevent data overfitting and overtraining on ANN (Dan Foresee and Hagan 1997). The use of ANNs involves two steps: first, the network is trained using a set of training data, and then it is tested using test data to see how well it can predict the future. In this study, the features of the network architecture of the ANN model are presented in Table 4. Table 5 contains the statistical data of the parameters that make up the inputs and output of the ANN model. Since the curing conditions are non-parametric, they are parametrically coded. The percentage of training/test was chosen as 85/15 according to the articles reviewed in the literature (SinghSandhu and Singh Salaria 2014; Hussain and AlAlili 2016).

Table 4 Properties of network architecture

Parameter	Model properties
Number of input factors	3
Number of output factors	1
Number of hidden layers (HL)	1
Number of neurons on HL	10
Training/test percentage	85/15
Number of epochs	100
Performance limit	10^{-6}
Training method	Supervised
Training algorithm	Bayesian regulariZsation
The activation function in the hidden layer	Non-linear (tansig)
The activation function in the output layer	Linear (purelin)

Table 5 Statistical properties of input and output parameters

	Parameter	Minimum	Maximum	Mean	Standard deviation
Inputs	RHA (kg)	0	100	50	70.7
	GBFS (kg)	0	150	75	106.1
	Curing conditions*	1	3	–	–
Output	28-day compressive strength (MPa)	92.3	119.9	106.1	19.5

* 1(water curing)−2(hot water curing)−3(steam curing)

3 Results and Discussions

3.1 Fresh Properties

Figure 3 presents the flow diameters of cementitious composites determined according to ASTM C1347. The flow diameter of cementitious composites varies between 213 and 255 mm. The highest flow diameter was obtained with 255 mm G10R0 mixture using 10% GBFS. The lowest flow diameter with a value of 213 mm was obtained in G5R10 mixture using 5% GBFS and 10% RHA. The

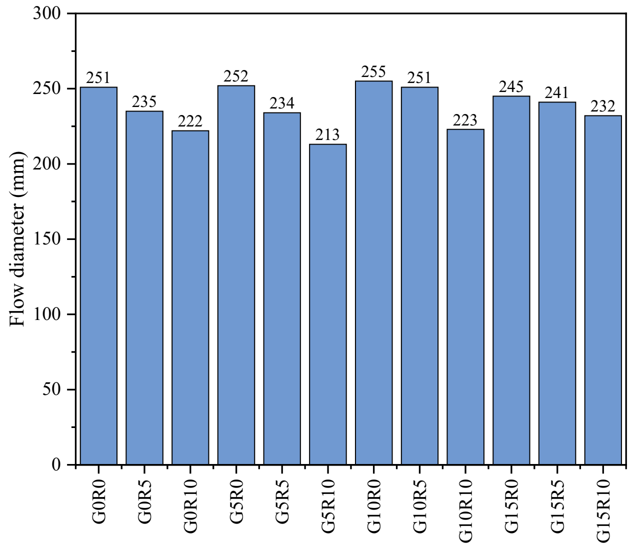

Fig. 3 Flow diameters of cementitious composites

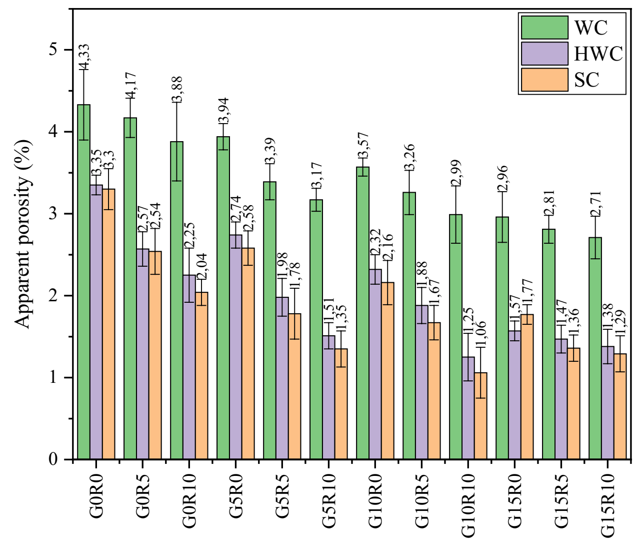

Fig. 4 Apparent porosity of cementitious composites

flow diameter of the G15R10 mixture, in which the most mineral additives were used (25%), decreased by approximately 8% compared to the reference mixture. The propagation diameter increased when 5 and 10% GBFS were used. Workability is partially improved as GBFS increases the paste volume in the mix. As the RHA content used in the mixtures increases, the workability decreases. The porous structure of RHA and the very high specific surface area led to a decrease in workability. However, the combined use of 15% GBFS and RHA reduced the workability loss. The flow diameter of the mixtures using 10% RHA generally decreased below 225 mm. Workability increases when GBFS is used at a low rate (5 and 10%). Because GBFS pushes the water remaining between the cement particles and fills them. The water from the cement particles increases the workability relatively with the lubricating effect.

Ahmed et al. reported that the flow diameter decreases as the RHA content increases. The reduction in flow diameter was explained by the high porosity of RHA (Ahmed et al. 2022). In cementitious composites, RHA considerably increases the water requirement. Therefore, the workability decreases at a fixed water content (Medina et al. 2018). Similar results were obtained in the study by Kaplan and Elmekahal (Kaplan and Salem Elmekahal 2021). Aldabagh et al. used up to 30% GBFS in self-compacting mortars. The diffusion diameter of the mixtures decreased slightly as the GBFS content increased (Aldabagh et al. 2022). Similar results were observed by Benli et al. (Benli et al. 2017). Murthy and Rao proved with SEM images that GBFS has an irregular and angular particle structure (Murthy and Rao 2016). The fact that GBFS has such a particle structure is another factor that reduces the workability of the mixtures.

3.2 Physical Properties

In Fig. 4, the apparent porosity values of the cementitious composites are shown. The porosities of the mixtures subject to different curing conditions are below 5%. The apparent porosities of cementitious composites subjected to WC range from 2.71 to 4.33%. The apparent porosities of the mixtures treated with HWC and SC showed similar properties. Applying HWC and SC considerably reduced the apparent porosity of the mixtures. For example, if HWC or SC were applied in the reference mixture, the apparent porosity was reduced by approximately 25%. The use of RHA in cementitious composites reduced the porosity. The apparent porosity of the water-cured G0R10 mixture decreased by 10.3% compared to the G0R0 Mixture. When HWC and SC were applied to this mixture, the porosity decreased by 32.9 and 38.2%, respectively. The apparent porosity of the WC-applied G15R10 mixture is reduced by 8.4% compared to the G15R0 mixture. The porosity decreased by 12.1% when HWC was applied to the same mixture and 27.1% when SC was applied. Applying a thermal curing method to the mixtures further reduces the apparent porosity. Since thermal cures accelerate the pozzolanic activity, they ensure that the microstructure is denser. Therefore, the apparent porosity of cementitious composites is greatly reduced. The porosity of cementitious composites treated with HWC and SC is less than 4%. Especially when thermal cure is applied to mixtures using 10% RHA, the porosity value generally falls below 2%. With the increase in GBFS content, the porosity value of the mixtures decreases. When 15% GBFS was used in WC-applied mixtures, the porosity decreased approximately 1.5 times. This ratio is approximately 2.6

times in SC-applied mixtures. GBFS was effective in reducing apparent porosity due to both its pozzolanic activity and its filler properties.

Sobrosa et al. have produced ceramic mixtures using up to 20% RHA. They observed that the porosity of the mixtures decreased as the RHA content increased (Sobrosa et al. 2017). Olutoge and Adesina stated that the porosity of cement mortars increased as the RHA content increased. This effect is explained by the porosity of RHA (Olutoge and Adesina 2019). Similar results were obtained by Pereira et al. (Pereira et al. 2013). Li et al. reduced the apparent porosities of the mixtures using GBFS up to 15% (Li et al. 2018). It was stated that the porosity decreased due to the pozzolanic activity of GBFS. Aprianti et al. found that the porosity of GBFS-containing mixtures decreased when hot water curing was applied (Aprianti et al. 2016). Malami and Kaloidas stated that curing conditions were highly effective on porosity (Malami et al. 1994). Similar results were obtained in this study as well.

The water absorption behavior of cementitious composites is given in Fig. 5. Applying thermal curing methods to the mixtures reduced the water absorption values as it intensified the microstructure. While the water absorption value of WC applied mixtures is more than 1%, the water absorption of HWC and SC applied mixtures is generally less than 1%. Water absorption decreased by 22.4% in the case of applying HWC to the G0R0 mixture, and by 29.7% in the case of applying SC. As the RHA content increases in cementitious composites, the water absorption values decrease. It consists of smaller particles than RHA cement. Therefore, water absorption decreases as it fills the spaces between the cement particles. For example, the water absorption of the G0R15 mixture, which was water cured, decreased by 27.1% compared to the G0R0 mixture. When SC was applied to the mixtures, this value was measured as 36.3%. Water absorption values also decrease when GBFS is used in cementitious composites. The water absorption of the G15R0 mixture, which was water cured, decreased by 27.6% compared to the G0R0 mixture. In mixtures applied with HWC, this value is 55%. RHA and GBFS greatly reduce porosity and water absorption due to their pozzolanic activity and smaller particle size than cement. Since thermal curing methods accelerate the pozzolanic activity, the water absorption values have generally decreased below 1%. Studies in the literature have also reported that pozzolans reduce water absorption (Pereira et al. 2013; Olutoge and Adesina 2019; Gencel et al. 2022).

As can be seen in Fig. 6, very clear differences can be seen between the hardened unit weights of the mixtures. Unit weights of water-cured cementitious composites vary between 2285 and 2336 kg/m^3. While the unit weight of HWC-treated mixtures is between 2285 and 2378 kg/m^3, it is between 2345 and 2440 kg/m^3 for SC-treated mixtures. Application of thermal curing methods to cementitious composites relatively increased unit weights. Such an effect has been observed because thermal curing methods increase the density of the microstructure. Increasing the content of RHA and GBFS in cementitious composites decreased the unit weights very little. Since the specific gravity of RHA and GBFS is lower than cement, unit weights tend to fall. It is observed that the unit weights of cementitious composites are generally more than 2300 kg/m^3. It was determined that the mixtures that applied SC cure had higher unit weight. The order of SC > HWC > WC was obtained among the unit weights. Unit weights of cementitious composites treated with HWC and WC are similar.

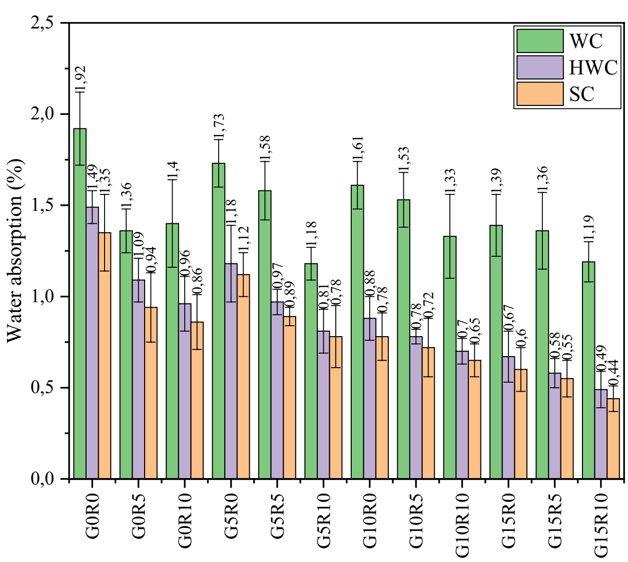

Fig. 5 Water absorption of cementitious composites

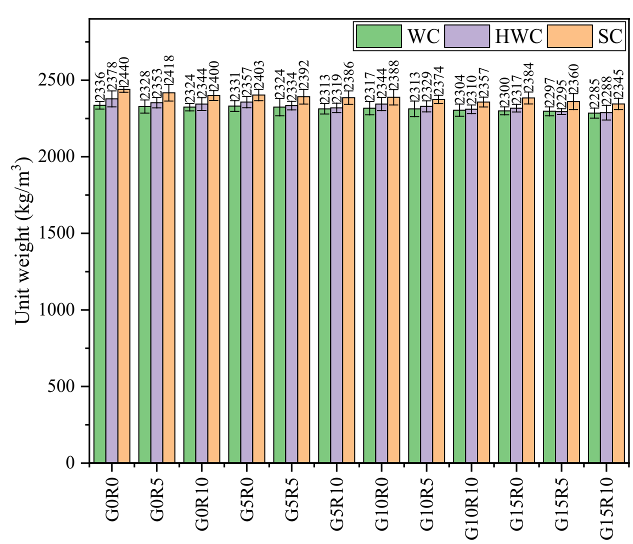

Fig. 6 Unit weight of cementitious composites

3.3 Mechanical Properties

As seen in Fig. 3a, the 3-day compressive strength of cementitious composites varies between 53.4 and 90.6 MPa. These results show that a compressive strength of more than 50 MPa can be obtained at early ages despite the use of pozzolan. The compressive strength of WC applied mixtures is between 53.4 and 75.6 MPa. Applying thermal cures such as HWC and SC to the mixtures greatly improves the early age strength. In particular, the compressive strength of SC applied mixtures varies between 68.4 and 90.6 MPa. If GBFS and RHA are used instead of cement in the mixtures, their 3-day compressive strength is relatively reduced. This is because the pozzolanic activity has not been completed yet. In addition, since the porosity of the hardened samples is quite low, they are very impenetrable. Therefore, even if thermal curing methods are applied to the mixtures, the strengths have decreased since steam or water cannot be transported to the sample's interior.

Seven-day compressive strengths of cementitious composites are presented in Fig. 7b. The 7-day compressive strength of the mixtures varies between 77 and 102.6 MPa. Compressive strengths of more than 100 MPa were obtained after 7 days of curing. However, values above

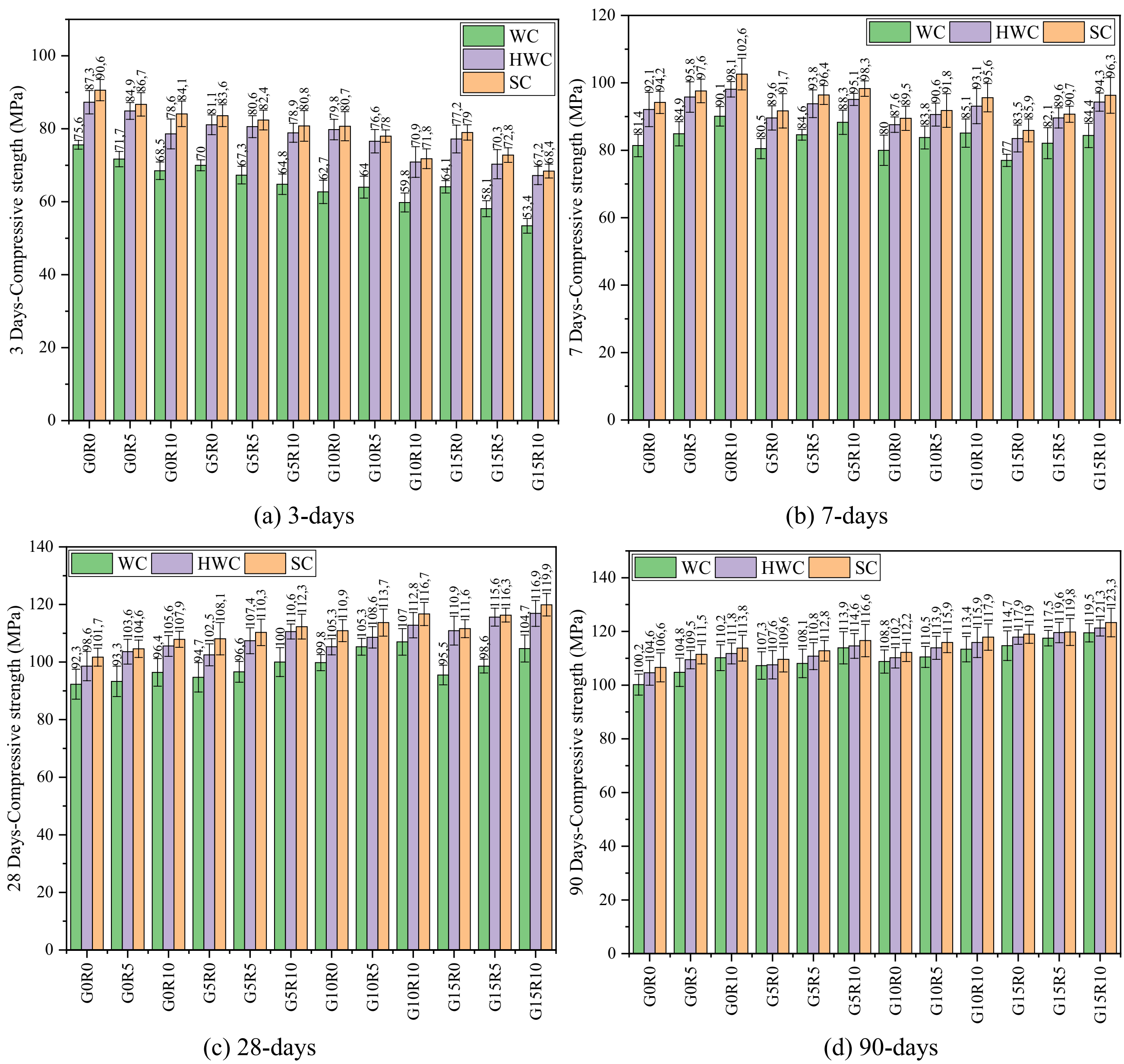

Fig. 7 Compressive strength of cementitious composites

100 MPa could not be obtained in WC-applied mixtures. Since thermal curing methods accelerate hydration and pozzolanic activity, the value of 100 MPa was exceeded. As the RHA content of the mixtures increased, the 7-day compressive strength increased. In particular, compressive strength of 102.6 MPa was achieved when SC was applied to the G0R10 mixture. The high SiO_2 content of RHA contributed positively to the pozzolanic activity. Since a high cement content is used in the mixtures, the combination of RHA + cement considerably increased the compressive strength. In this process, the Ca/Si ratio is also effective. However, as the GBFS content in the mixtures increased, the compressive strength generally decreased. Strength loss due to GBFS in mixtures is negligible.

The 28-day compressive strength of cementitious composites is between 92.3 and 119.9 MPa (Fig. 7c). Compressive strength exceeds 100 MPa if RHA is used in mixtures where water cure is applied and GBFS is at least 10%. For example; The 28-day compressive strength of the water-cured G10R10 mixture increased by approximately 16% compared to the G0R0 mixture. The compressive strength of the mixtures applied HWC and SC exceeded 100 MPa. The highest compressive strengths were obtained when HWC and SC were applied to the G15R10 mixture. The compressive strength of the SC-applied G15R10 mixture increased by about 30% compared to the WC-applied G0R0 mixture. Using pozzolan's thermal curing methods in the mixtures positively contributed to the compressive strength. Using 15% GBFS in water-cured mixtures reduced the compressive strength relatively. However, as the GBFS content increases, the compressive strength increases in thermally cured mixtures. This result again reveals the need for the thermal curing of pozzolans.

As seen in Fig. 7d, the 90-day compressive strengths of the mixtures vary between 100.2 and 123.3 MPa. The 90-day compressive strength of the WC-applied mixtures exceeded 100 MPa. The 90-day compressive strength of the WC-applied G15R10 mixture increased by approximately 20% compared to the G0R0 mixture. Since the pozzolanic activity progresses slowly in the normal water cure, the actual strength gain was observed on the 90th day. Thermal curing methods relatively increased the compressive strength of cementitious composites. In case of applying HWC and SC to the G0R0 mixture, the compressive strength increased by around 4 and 6.5%, respectively, compared to the water-cured G0R0 mixture. Increasing the content of RHA and GBFS used in the mixtures generally increased the compressive strength. In addition to the pozzolanic activity feature of pozzolans, the filler feature also increases the compressive strength. In addition, as pozzolans intensify the microstructure, the strength properties are improved. However, this effect can be observed mainly at the age of 28 and above.

Zhang et al. obtained compressive strengths of more than 100 MPa in mixtures using RHA (Zhang et al. 2021). Gastaldini et al. obtained a compressive strength of approximately 72.5 MPa at 28 days using 20% RHA (Gastaldini et al. 2007). Salas et al. recommend 5–10% RHA content to increase compressive strength (Salas et al. 2009). Kunchariyakun et al. reported that as RHA increases the water requirement, it decreases the compressive strength (Kunchariyakun et al. 2015). However, the high SiO_2 content and specific surface area of RHA are very effective in increasing the compressive strength. However, thermal curing methods such as hot water curing of mixtures using pozzolana improve the compressive strength considerably (Gomathi and Sivakumar 2015; Shahane and Patel 2021). Similarly, hot water curing contributes to the development of strength in GBFS mixtures (Federowicz et al. 2020).

As seen in Fig. 8, the flexural strength of cementitious composites exhibits a behavior parallel to the compressive strength. 3-day flexural strengths of water-cured mixtures vary between 7.2 and 9.8 MPa. The flexural strength of mixtures applied with HWC varies between 10.9 and 12.9 MPa, and mixtures with SC applied between 11.2 and 14.6 MPa. As the RHA content increases in water-cured mixtures, the flexural strength (3-days) decreases. However, when thermal curing methods such as HWC and SC are applied, flexural strength generally increases as the RHA content increases. Because thermal curing methods accelerate the pozzolanic activity, flexural strength improves. In addition, using GBFS up to 10% in thermal cure methods also increases the 3-day flexural strengths.

As the RHA content increased, the 7-day flexural strengths generally decreased in the water-cured mixtures (Fig. 8b). Similarly, such an effect was observed as the GBFS content increased. However, as the GBFS and RHA content increased, the flexural strength of the mixtures applied HWC and SC increased. The 7-day flexural strength of the mixtures treated with HWC and SC exceeded 11 MPa. Especially in the case of applying HWC and SC in the G15R10 mixture, more than 15 MPa flexural strength was obtained on the 7th day.

As seen in Fig. 8c, the 28-day flexural strength of all cementitious composites exceeded 10 MPa. In addition, it is observed that the flexural strength increased as the RHA and GBFS content increased on the 28th day. The flexural strength of WC applied mixtures is between 12.1 and 14.7 MPa. The flexural strength of the WC-applied G15R10 mixture increased by approximately 18% compared to the G0R0 mixture. In SC and HWC applied mixtures, this value was measured as 26.6 and 25.5%, respectively. Although the amount of cement was reduced by 25%, flexural strength was increased. Since the microstructure is more concentrated in thermal curing methods, the strength gain is higher. Flexural strength of more than 17 MPa was obtained when thermal

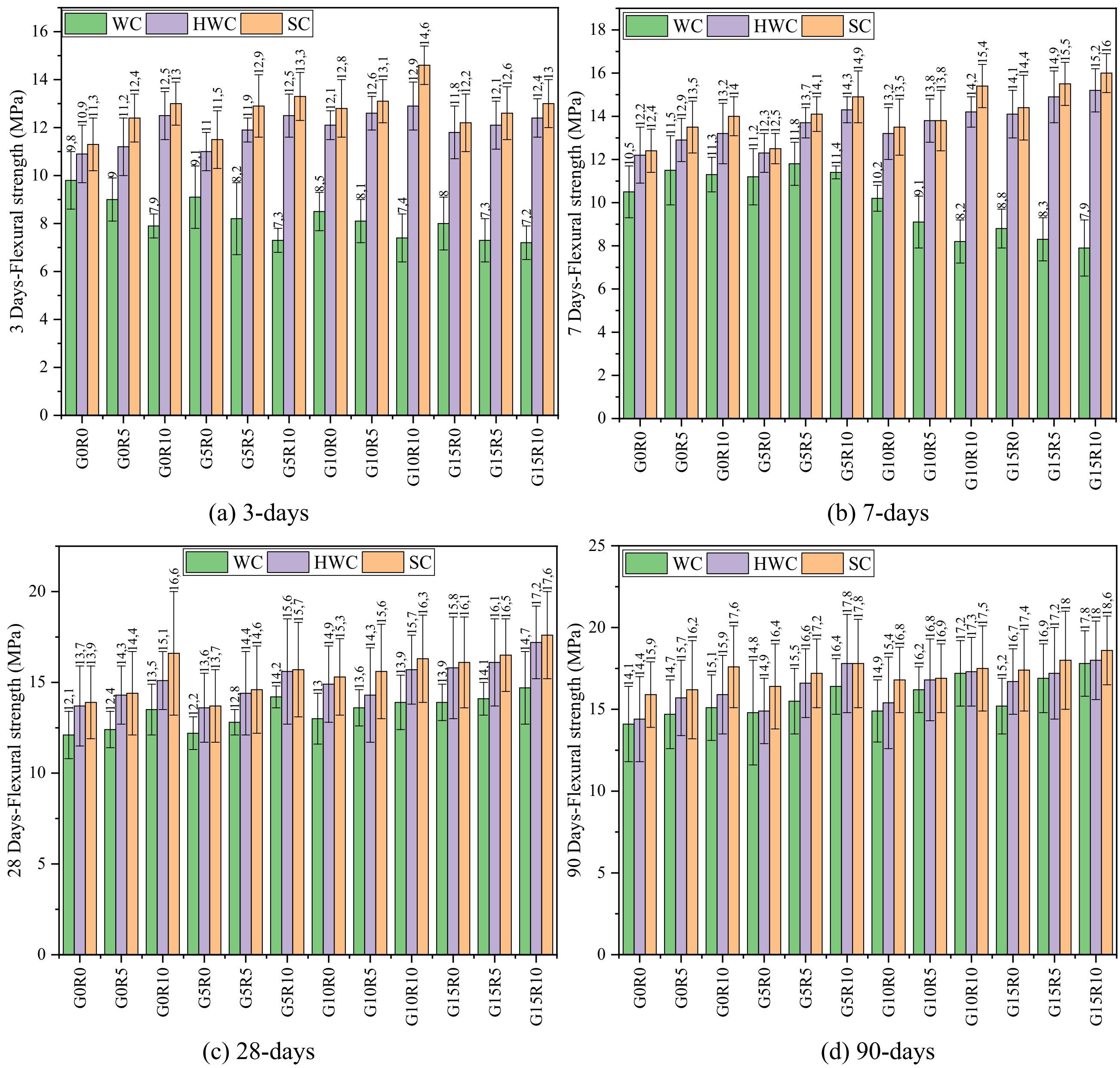

Fig. 8 Flexural strength of cementitious composites

curing methods were used, especially in the mixture of G15R10, where the most pozzolana was used.

As seen in Fig. 8d, the flexural strengths generally exceeded 15 MPa on the 90st day due to the pozzolanic activity. A flexural strength of approximately 19 MPa at day 90 in the SC-applied G15R10 mixture. The flexural strength of the SC-applied G15R10 mixture increased by about 32% compared to the water-cured G0R0 mixture. This result shows that the cement substitution rate can increase significantly. In this way, it is possible to produce more sustainable mixtures. When the effect of curing conditions at all ages was examined, the order of SC > HWC > WC was obtained. In addition, while RHA and GBFS content generally decreased flexural strength at 3 and 7 days of age, the opposite effect was observed at 28 and 90 days.

In Fig. 9, the changes in compressive strength were observed based on the reference mixture (G0R0). If the compressive strength ratio falls below 1, it means strength loss. If it rises above 1, it means strength gain. Since GBFS and RHA are used in all mixtures (except the reference mixture) according to their 3-day compressive strength, a loss of compressive strength has occurred. The G15R10 mixture, in which water cure was applied and the most pozzolan was used, achieved 71% strength of the reference mixture in

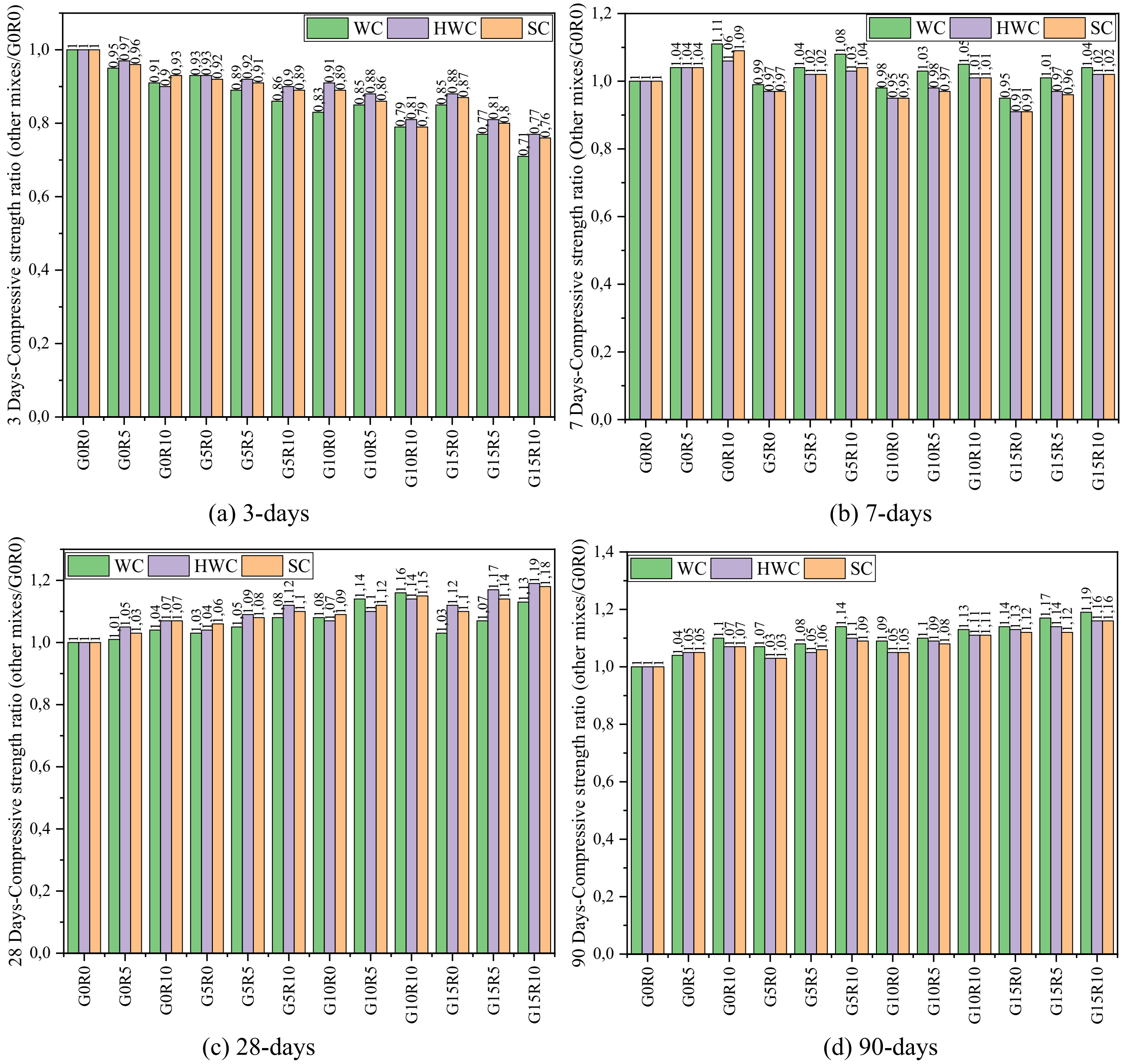

Fig. 9 Compressive strength ratio of cementitious composites

3 days. On the other hand, G0R5 was the mixture that came closest to (> %95) the reference mixture on the 3rd day. On the 7th day, increases were observed in the compressive strength of G0R5 and G0R10 mixtures (Fig. 9b). In addition, similar results were observed for mixtures of G5R10, G10R10 and G15R10. The use of 10% RHA in cementitious composites generally increased the compressive strength ratio. The highest strength increase (approximately 19%) was observed in the G15R10 mixture applied with HWC at 28 days (Fig. 9c). When the G0R5 mixture was subjected to water curing, the compressive strength increased by 1%. As the pozzolan content increases, using thermal curing methods is more effective in increasing the compressive strength. Similar results are also observed in the 90-day compressive strength ratio (Fig. 9d). On the 90th day, the increase in strength varies between 4 and 19% according to different curing conditions. Application of WC only in mixtures with GBFS increases strength. However, if RHA is used, it should be used in thermal curing methods. GBFS shows hydraulic properties due to its high CaO content. Therefore, it can increase the compressive strength in water curing. However, the high SiO_2 content of RHA highlights its pozzolanic feature. Applying thermal curing for the pozzolanic reaction between CaO and SiO_2 contributes to the

strength development. These results show the importance of Ca/Si ratio on strength development in cementitious systems. As the SiO_2 content increases, the Ca/Si ratio will decrease. Therefore, it will be more efficient to use thermal curing methods in low Ca/Si based pastes.

The use of GBFS and RHA in 3-day water cure mixtures increases the compressive/flexural strength ratio. However, the opposite effect was observed in thermal cured mixtures (Fig. 10a). As seen in Fig. 10b, the compression/flexural ratio of the mixtures with GBFS and RHA applied with HWC and SC decreased. The compressive/flexural strength ratio of the G15R10 mixture, which is water cured, has increased by approximately 38% compared to the G0R0 mixture. HWC and SC application decreased the compressive/flexural strength ratio in 29- and 90-day mixtures (Fig. 10c, d). However, the application of water cures generally increases this rate. Increasing the RHA content in the mixtures generally decreased the compressive strength ratio. Because RHA increases the brittleness of cementitious composites. Therefore, this ratio decreased as the brittleness increased. As the compressive/flexural strength ratio gives information about the toughness in cementitious systems, it is desired that this ratio be high (Parghi and Shahria Alam 2016; Soltaninejad et al. 2021).

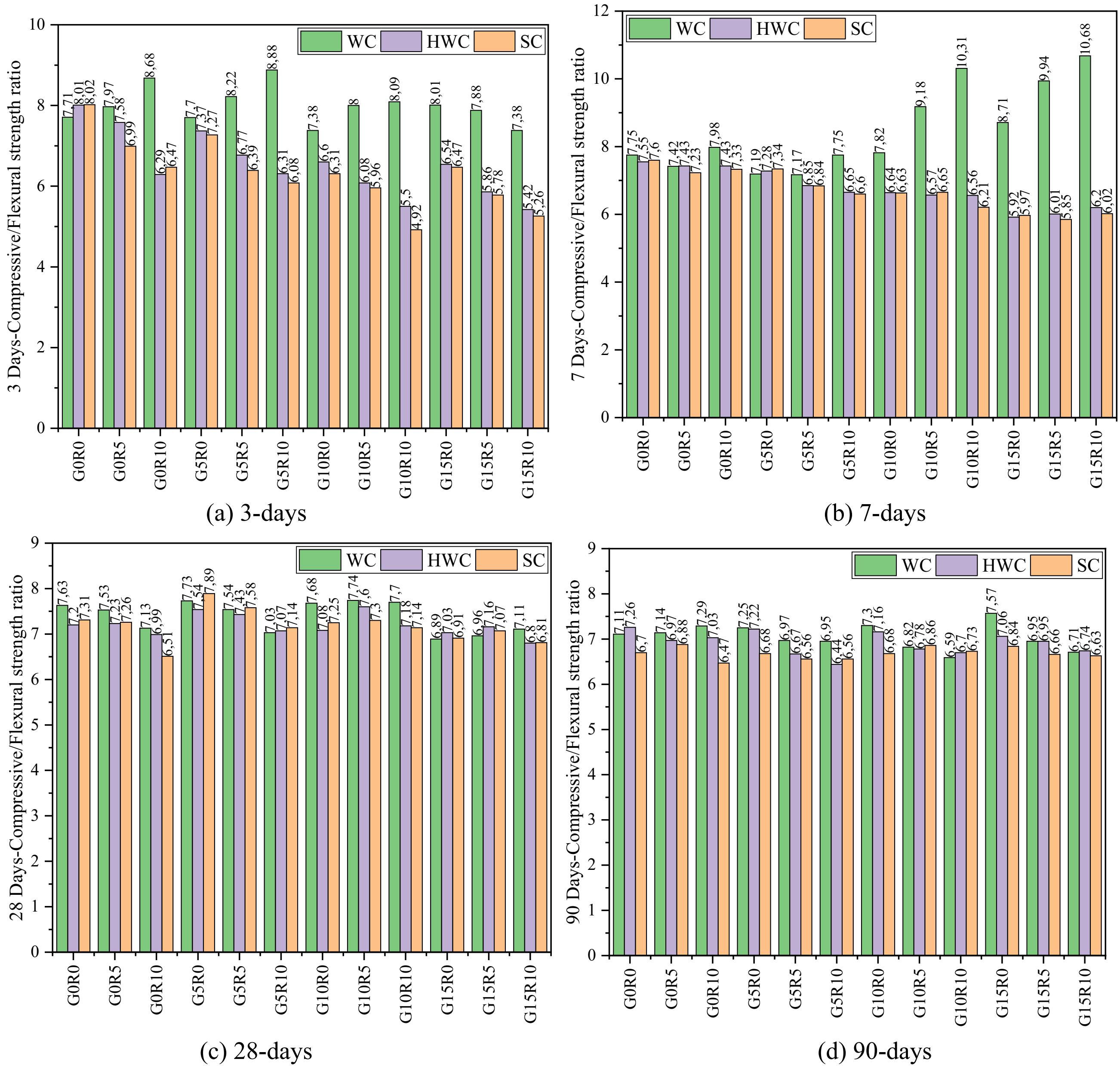

Fig. 10 Compressive/flexural strength ratio of cementitious composites

In the study conducted by Öz et al., the compressive/flexural strength ratio of mixtures with a compressive strength of more than 100 MPa is between 12.3 and 18 (Öz et al. 2022). This study's compressive/flexural strength ratios are less than 10.

As seen in Fig. 11a, the 90-day compressive strength increases as the apparent porosity of cementitious composites decrease under all curing conditions. The porosities of the mixtures cured in HWC and SC are relatively lower. Accordingly, the compressive strength of these mixtures is higher. The apparent porosities of WC-cured mixtures are usually greater than 3%. As seen in Fig. 11b, the compressive strength increases as the unit weight of the mixtures decreases. The unit weight of the mixtures decreases as the GBFS and RHA content increases. Because the specific gravity of GBFS and RHA is lower than cement. Pozzolans such as GBFS and RHA increase compressive strength due to pozzolanic activity. Therefore, as the GBFS and RHA content increase, the unit weights decrease while the compressive strength increases. In addition, it is observed that thermal curing methods increase the unit weight relatively because they intensify the microstructure by reducing the porosity.

As seen in Fig. 12, the flexural strength of cementitious composites increases as the compressive strength increases in all curing conditions. Strong correlation values ($R^2 > 0.75$) were observed between compressive and flexural strength. Compressive strength of about 125 MPa and flexural strength of 19 MPa were observed in cementitious composites. A ratio of 1/15 was obtained between compressive and flexural strength. In terms of mechanical properties, the order SC > HWC > WC was obtained under curing conditions.

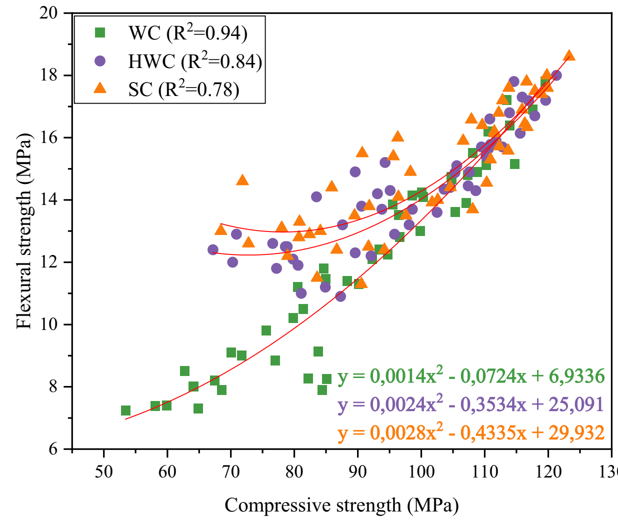

Fig. 12 Relationship between compressive and flexural strength

3.4 Microstructures

Figure 13 presents the microstructure properties of G0R0 and G15R10 mixtures at different curing conditions. SEM analyzes of the samples were performed after 90 days of cure. As seen in the SEM images, it is seen that a dense CSH structure is formed in the microstructure. A dense microstructure was observed in the mixtures subjected to water cure after 90 days. Reticular CSH gels are observed in

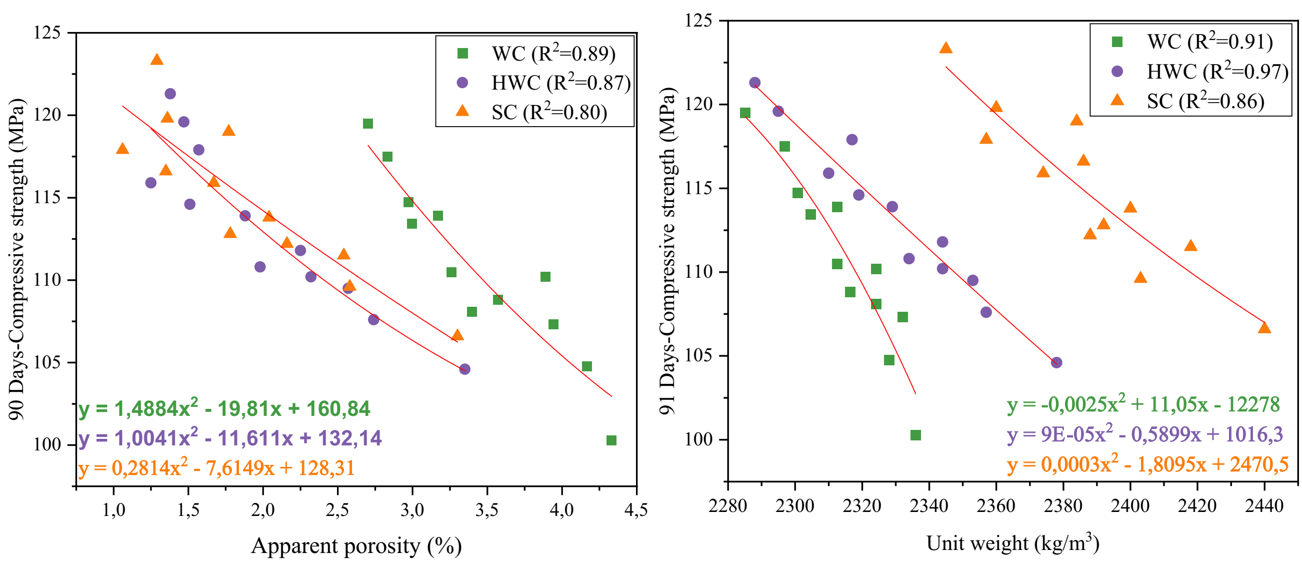

(a) Porosity-Compressive strength

(b) Unit weight-Compressive strength

Fig. 11 Relationship between compressive strength and physical properties

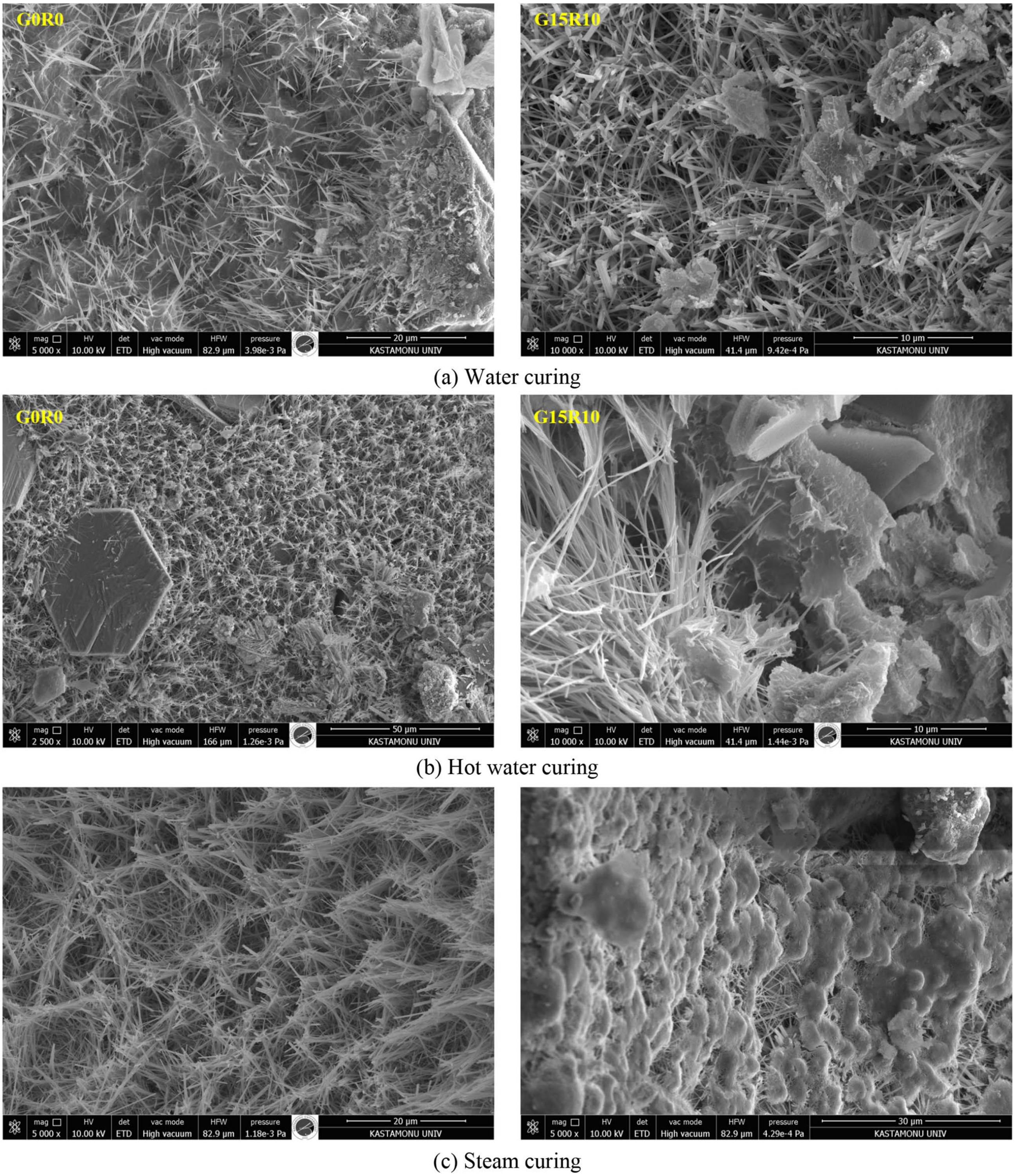

Fig. 13 SEM images of cementitious composites

the microstructure. In addition, very few microcracks were observed in the matrix (Fig. 13a). Needle-like CSH gels are frequently observed in mixtures with hot water cures. Hexagonal CH plaques were observed in the G0R0 mixture, where pozzolans such as GBFS and RHA were not used. The approximate size of the CH plate is 20 µm (Fig. 13b). Similar microstructure images were also observed in mixtures treated with steam curing (Fig. 13c). It was determined that dense CSH gels were formed in the microstructure and that the gels were in the form of needles. These dense CSH gels formed in the microstructure greatly increased the strength of cementitious composites.

3.5 ANN Model Results

The regression results of the developed ANN model are given in Fig. 14. R^2 values for training and test data were obtained as 0.93 and 0.95, respectively. These results show that the training and testing were quite successful. In addition, the R^2 value of the whole model was obtained as 0.93. It has been determined that 28-day compressive strength can be obtained with very high accuracy using GBFS and RHA content and curing conditions.

Figure 15 illustrates the ANN training's error reduction method, which offers the best illustration possible of the model training procedure. The figure shows the network training error as a blue line and the test error as a red line. The training is finished when the verification error reaches the predetermined objective or stops declining.

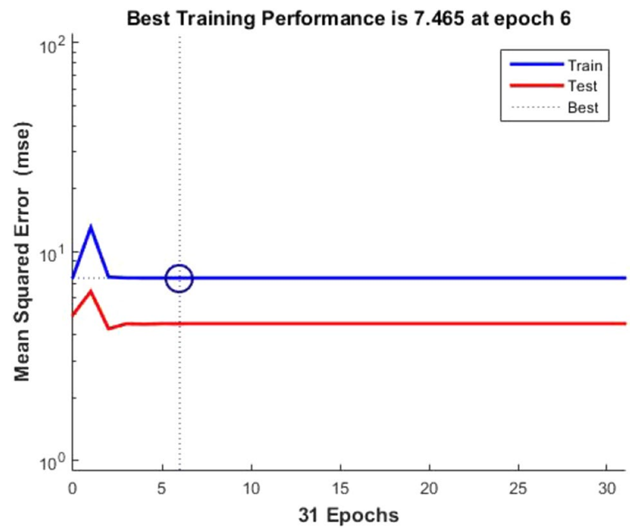

Fig. 15 MSE of Training and testing

Fig. 14 Regression results of the ANN model

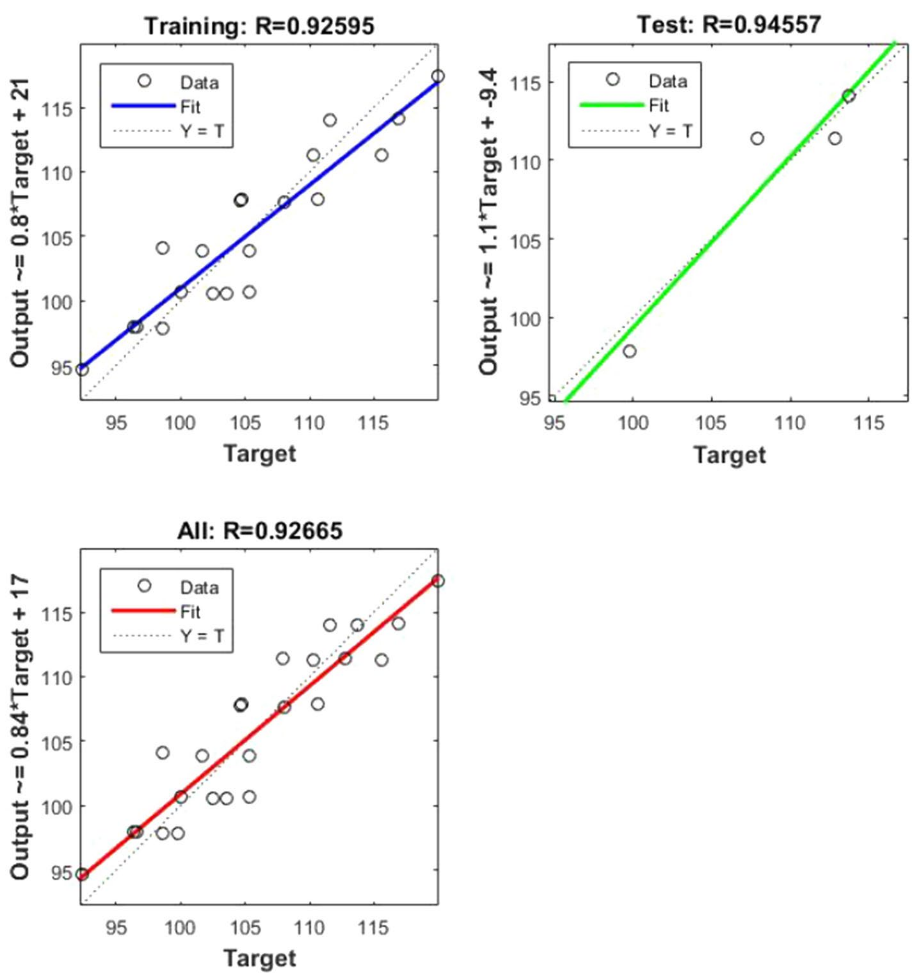

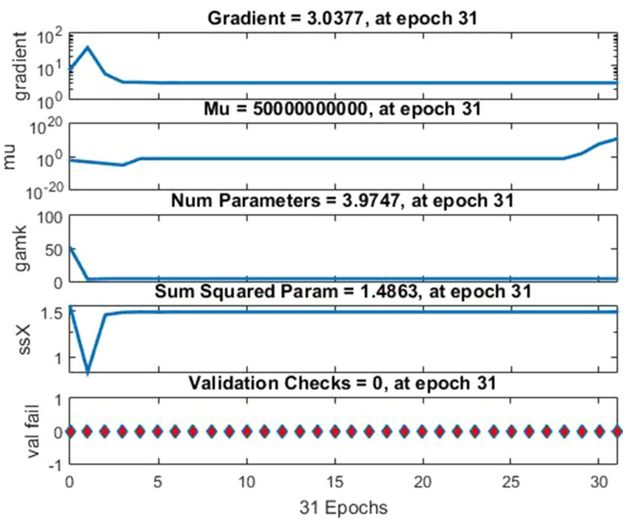

Fig. 16 The training state for the ANN model

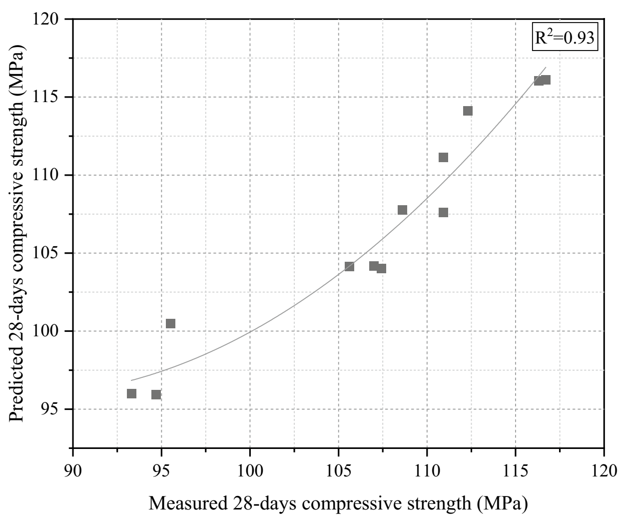

Fig. 17 Comparison between the predicted and measured 28 days-compressive strength by the ANN model for test data

The figure shows that the best training performance was achieved after 6 epochs.

Figure 16 shows the training status of the ANN model. The training of the ANN model has been completed in 31 epochs. Also, there was no recurrence due to any errors.

As can be seen in Fig. 17, it has been observed that the measured and estimated values are quite close to each other as a result of the simulation performed. Thanks to the developed model, the 28-day compressive strength can be determined largely by using the GBFS and RHA content and curing conditions. It will be possible to decide on the optimum mixing ratios with the Bayesian algorithm.

4 Conclusions

- The workability decreased as the RHA content increased in cementitious composites. Workability is improved if up to 10% GBFS is used.
- As the content of RHA and GBFS increased, the mixtures' water absorption and apparent porosity decreased. In addition, the use of thermal curing methods (HWC or SC) significantly reduced water absorption and apparent porosity.
- RHA and GBFS have no obvious effect on unit weight. However, since thermal curing methods intensified the microstructure, unit weights increased.
- Increasing the content of RHA and GBFS decreased the 3-day compressive strength. However, the 7-day compressive strength increased with the increase in RHA content. As both RHA and GBFS content increased, 28 and 90-day compressive strengths increased. Similar results were observed in flexural strengths. Steam curing application increases compressive and flexural strength more than hot water and normal water curing.
- The low w/c or w/b ratio observed a dense microstructure in SEM images. Needle-like CSH gels and hexagonal-shaped CH plaques were observed.
- A highly accurate ANN model has been developed. It has been found that optimum material amounts and curing conditions can be determined using the algorithm.
- As a result, cementitious composites with high early-age strength could be obtained with 25% cement savings by using RHA and GBFS. It has been shown that more sustainable and durable mixtures can be obtained with the proposed mixtures.

References

Ahmed A, Ameer S, Abbas S et al (2022) Effectiveness of ternary blend incorporating rice husk ash, silica fume, and cement in preparing ASR resilient concrete. Materials 15:2125. https://doi.org/10.3390/MA15062125

Aldabagh IS, Abed JM, Khaleel BA, Hamah Sor N (2022) Influence of water quality and slag on the development of mechanical properties of self-compacting mortar. Mater Today Proc 57:892–897. https://doi.org/10.1016/J.MATPR.2022.02.575

Angulo-Ramirez DE, Mejía De Gutiérrez R, Valencia-Saavedra WG et al (2019) Carbonation of hybrid concrete with high blast furnace slag content and its impact on structural steel corrosion. Mater Constr. https://doi.org/10.3989/mc.2019.05418

Aprianti E, Shafigh P, Zawawi R, Abu Hassan ZF (2016) Introducing an effective curing method for mortar containing high volume cementitious materials. Constr Build Mater 107:365–377. https://doi.org/10.1016/j.conbuildmat.2015.12.100

Atici U, Ersoy A (2008) Evaluation of destruction specific energy of fly ash and slag admixed concrete interlocking paving blocks

(CIPB). Constr Build Mater 22:1507–1514. https://doi.org/10.1016/j.conbuildmat.2007.03.028

Bayraktar OY (2019) The possibility of fly ash and blast furnace slag disposal by using these environmental wastes as substitutes in Portland cement. Environ Monit Assess. https://doi.org/10.1007/s10661-019-7741-4

Bayraktar OY (2021) Possibilities of disposing silica fume and waste glass powder, which are environmental wastes, by using as a substitute for Portland cement. Environ Sci Pollut Res 28:16843–16854. https://doi.org/10.1007/s11356-020-12195-9

Bayraktar OY, Citoglu GS, Belgin CM et al (2019) Investigation of effect of brick DFST and silica FFME on the properties of Portland cement mortar. Fresenius Environ Bull 28:7823–7832

Benli A, Karataş M, Bakir Y (2017) An experimental study of different curing regimes on the mechanical properties and sorptivity of self-compacting mortars with fly ash and silica fume. Constr Build Mater 144:552–562. https://doi.org/10.1016/j.conbuildmat.2017.03.228

Boubekeur T, Boulekbache B, Aoudjane K et al (2019) Prediction of the durability performance of ternary cement containing limestone powder and ground granulated blast furnace slag. Constr Build Mater 209:215–221. https://doi.org/10.1016/j.conbuildmat.2019.03.120

Chang I, Lee M, Cho GC (2019) Global CO_2 emission-related geotechnical engineering hazards and the mission for sustainable geotechnical engineering. Energies 12:2567

Cheah CB, Liew JJ, Khaw Le Ping K et al (2022) Properties of ternary blended cement containing ground granulated blast furnace slag and ground coal bottom ash. Constr Build Mater. https://doi.org/10.1016/j.conbuildmat.2021.125249

Cordeiro GC, Toledo Filho RD, Fairbairn DMR, E, (2009) Use of ultrafine rice husk ash with high-carbon content as pozzolan in high performance concrete. Mater Struct Constr 42:983–992. https://doi.org/10.1617/s11527-008-9437-z

Crossin E (2015) The greenhouse gas implications of using ground granulated blast furnace slag as a cement substitute. J Clean Prod 95:101–108. https://doi.org/10.1016/j.jclepro.2015.02.082

Çelik DN, Demircan RK, Shi J et al (2023) The engineering properties of high strength mortars incorporating juniper seed ash calcined at different temperatures: comparison with other SCMs. Powder Technol. https://doi.org/10.1016/j.powtec.2023.118474

Dan Foresee F, Hagan MT (1997) Gauss-Newton approximation to Bayesian learning. In: IEEE international conference on neural networks—conference proceedings, pp 1930–1935

De Silva GHMJS, Perera BVA (2018) Effect of waste rice husk ash (RHA) on structural, thermal and acoustic properties of fired clay bricks. J Build Eng 18:252–259. https://doi.org/10.1016/j.jobe.2018.03.019

Elsunousi AAM, Sevik H, Cetin M et al (2021) Periodical and regional change of particulate matter and CO_2 concentration in Misurata. Environ Monit Assess. https://doi.org/10.1007/s10661-021-09478-0

Federowicz K, Figueiredo VA, Al-Kroom H et al (2020) The effects of temperature curing on the strength development, transport properties, and freeze-thaw resistance of blast furnace slag cement mortars modified with nanosilica. Materials 13:1–15. https://doi.org/10.3390/ma13245800

Ganesh AC, Muthukannan M (2021) Development of high performance sustainable optimized fiber reinforced geopolymer concrete and prediction of compressive strength. J Clean Prod. https://doi.org/10.1016/j.jclepro.2020.124543

Gastaldini ALG, Isaia GC, Gomes NS, Sperb JEK (2007) Chloride penetration and carbonation in concrete with rice husk ash and chemical activators. Cem Concr Compos. https://doi.org/10.1016/j.cemconcomp.2006.11.010

Gencel O, Nodehi M, Yavuz Bayraktar O et al (2022) Basalt fiber-reinforced foam concrete containing silica fume: an experimental study. Constr Build Mater. https://doi.org/10.1016/j.conbuildmat.2022.126861

Ghorbani S, Sun Y, Mohan MK, Matthys S (2023) Effect of copper and stainless steel slags on fresh, mechanical and pore structure properties of alkali activated ground granulated blast furnace slag. Case Stud Constr Mater. https://doi.org/10.1016/j.cscm.2023.e01981

Gomathi P, Sivakumar A (2015) Accelerated curing effects on the mechanical performance of cold bonded and sintered fly ash aggregate concrete. Constr Build Mater 77:276–287. https://doi.org/10.1016/j.conbuildmat.2014.12.108

Gupta V, Chai HK, Lu Y, Chaudhary S (2020) A state of the art review to enhance the industrial scale waste utilization in sustainable unfired bricks. Constr Build Mater 254:119220

Hakeem IY, Akter Hosen M, Tayeh BA, Alhamami A (2023) Innovative Ultra-High Performance Concrete (UHPC) Incorporating oil ash and electric arc furnace dust. Case Stud Constr Mater. https://doi.org/10.1016/j.cscm.2023.e01843

Han SH, Jun Y, Kim JH (2022) The use of alkaline CO_2 solvent for the CO_2 curing of blast-furnace slag mortar. Constr Build Mater 342:127977. https://doi.org/10.1016/J.CONBUILDMAT.2022.127977

Hussain S, AlAlili A (2016) Online sequential learning of neural networks in solar radiation modeling using hybrid Bayesian hierarchical approach. J Sol Energy Eng Trans ASME. https://doi.org/10.1115/1.4034907

Jakhrani SH, Ryou JS, Rehman AU et al (2019) Prevention of autogenous shrinkage in high-strength mortars with saturated tea waste particles. Materials. https://doi.org/10.3390/ma12172654

Jamil M, Khan MNN, Karim MR et al (2016) Physical and chemical contributions of Rice Husk Ash on the properties of mortar. Constr Build Mater. https://doi.org/10.1016/j.conbuildmat.2016.10.029

Jittin V, Bahurudeen A, Ajinkya SD (2020) Utilisation of rice husk ash for cleaner production of different construction products. J Clean Prod 263:121578

Kanthe VN (2021) Effect of superplasticizer on strength and durability of rice husk ash concrete. Iran J Energy Environ 12:204–208. https://doi.org/10.5829/ijee.2021.12.03.04

Kaplan G, Salem Elmekahal MA (2021) Microstructure and durability properties of lightweight and high-performance sustainable cement-based composites with rice husk ash. Environ Sci Pollut Res 28:52936–52962. https://doi.org/10.1007/s11356-021-14489-y

Kaplan G, Yaprak H, Memiş S, Alnkaa A (2019) Artificial neural network estimation of the effect of varying curing conditions and cement type on hardened concrete properties. Buildings. https://doi.org/10.3390/buildings9010010

Kaplan G, Yildizel SA, Memiş S, Öztürk AU (2018) The optimization of calcareous fly ash-added cement containing grinding aids and strength-improving additives. Adv Civ Eng. https://doi.org/10.1155/2018/8917059

Kramer HD, Daronco AS, de Vargas AS et al (2023) Effect of rice husk ash on the mechanical properties and microstructure of concrete subjected to high temperatures. J Mater Civ Eng. https://doi.org/10.1061/(asce)mt.1943-5533.0004664

Kunchariyakun K, Asavapisit S, Sombatsompop K (2015) Properties of autoclaved aerated concrete incorporating rice husk ash as partial replacement for fine aggregate. Cem Concr Compos. https://doi.org/10.1016/j.cemconcomp.2014.07.021

Lau CK, Lee H, Vimonsatit V et al (2019) Abrasion resistance behaviour of fly ash based geopolymer using nanoindentation and artificial neural network. Constr Build Mater 212:635–644. https://doi.org/10.1016/j.conbuildmat.2019.04.021

Li G, Zhang A, Song Z et al (2018) Ground granulated blast furnace slag effect on the durability of ternary cementitious system exposed to combined attack of chloride and sulfate. Constr Build Mater 158:640–648. https://doi.org/10.1016/j.conbuildmat.2017.10.062

Li P, Jiang J, Liu G, Ren Z (2022) Physical, mechanical, thermal and sustainable properties of UHPC with converter steel slag aggregates. Case Stud Constr Mater. https://doi.org/10.1016/j.cscm.2022.e01458

Lim JS, Cheah CB, Ramli MB (2019) The setting behavior, mechanical properties and drying shrinkage of ternary blended concrete containing granite quarry dust and processed steel slag aggregate. Constr Build Mater 215:447–461. https://doi.org/10.1016/j.conbuildmat.2019.04.162

Lippiatt N, Ling TC, Pan SY (2020) Towards carbon-neutral construction materials: carbonation of cement-based materials and the future perspective. J Build Eng 28:101062

Maddalena R, Roberts JJ, Hamilton A (2018) Can Portland cement be replaced by low-carbon alternative materials? A study on the thermal properties and carbon emissions of innovative cements. J Clean Prod 186:933–942. https://doi.org/10.1016/j.jclepro.2018.02.138

Malami C, Kaloidas V, Batis G, Kouloumbi N (1994) Carbonation and porosity of mortar specimens with pozzolanic and hydraulic cement admixtures. Cem Concr Res 24:1444–1454. https://doi.org/10.1016/0008-8846(94)90158-9

Medina C, Sáez del Bosque IF, Frías M, Sánchez de Rojas MI (2018) Design and characterisation of ternary cements containing rice husk ash and fly ash. Constr Build Mater 187:65–76. https://doi.org/10.1016/j.conbuildmat.2018.07.174

Miyandehi BM, Feizbakhsh A, Yazdi MA et al (2016) Performance and properties of mortar mixed with nano-CuO and rice husk ash. Cem Concr Compos 74:225–235. https://doi.org/10.1016/j.cemconcomp.2016.10.006

Moayedi H, Aghel B, Abdullahi MM et al (2019) Applications of rice husk ash as green and sustainable biomass. J Clean Prod 237:117851

Muntohar AS (2002) Utilization of uncontrolled burnt rice husk ash in soil improvement. Civ Eng Dimens 4:100–105

Murthy IN, Rao JB (2016) Investigations on physical and chemical properties of high silica sand, Fe–Cr slag and blast furnace slag for foundry applications. Procedia Environ Sci 35:583–596. https://doi.org/10.1016/j.proenv.2016.07.045

Nasiru S, Jiang L, Yu L et al (2021) Properties of cement mortar containing recycled glass and rice husk ash. Constr Build Mater. https://doi.org/10.1016/j.conbuildmat.2021.123900

Nduka DO, Olawuyi BJ, Fagbenle OI, Fonteboa BG (2022) Assessment of the durability dynamics of high-performance concrete blended with a fibrous rice husk ash. Crystals. https://doi.org/10.3390/cryst12010075

Okwu MO, Tartibu LK (2021) Artificial neural network. In: Studies in computational intelligence, pp 133–145

Olutoge FA, Adesina PA (2019) Effects of rice husk ash prepared from charcoal-powered incinerator on the strength and durability properties of concrete. Constr Build Mater. https://doi.org/10.1016/j.conbuildmat.2018.11.138

Öz A, Bayrak B, Kavaz E et al (2022) The radiation shielding and microstructure properties of quartzic and metakaolin based geopolymer concrete. Constr Build Mater 342:127923. https://doi.org/10.1016/J.CONBUILDMAT.2022.127923

Parghi A, Shahria Alam M (2016) Effects of curing regimes on the mechanical properties and durability of polymer-modified mortars—an experimental investigation. J Sustain Cem Mater 5:324–347. https://doi.org/10.1080/21650373.2015.1124812

Pereira CL, Savastano H, Payá J et al (2013) Use of highly reactive rice husk ash in the production of cement matrix reinforced with green coconut fiber. Ind Crops Prod 49:88–96

Razvi S, Saatcioglu M (1999) Confinement model for high-strength concrete. J Struct Eng 125:281–289. https://doi.org/10.1061/(asce)0733-9445(1999)125:3(281)

Rodríguez De Sensale G (2010) Effect of rice-husk ash on durability of cementitious materials. Cem Concr Compos 32:718–725. https://doi.org/10.1016/j.cemconcomp.2010.07.008

Salas A, Delvasto S, de Gutierrez RM, Lange D (2009) Comparison of two processes for treating rice husk ash for use in high performance concrete. Cem Concr Res 39:773–778. https://doi.org/10.1016/j.cemconres.2009.05.006

Sarıdemir M, Çelikten S, Çiflikli M, Karahancer M (2021) Influence of calcined diatomite content and elevated temperatures on the properties of high strength mortars produced with basalt sand. Struct Concr 22:E273–E290. https://doi.org/10.1002/suco.202000063

Sarıdemir M, Çelikten S, Yıldırım A (2020) Mechanical and microstructural properties of calcined diatomite powder modified high strength mortars at ambient and high temperatures. Adv Powder Technol. https://doi.org/10.1016/j.apt.2020.05.024

Selvaranjan K, Navaratnam S, Gamage JCPH et al (2021) Thermal and environmental impact analysis of rice husk ash-based mortar as insulating wall plaster. Constr Build Mater. https://doi.org/10.1016/j.conbuildmat.2021.122744

Sevik H, Cetin M, Guney K, Belkayali N (2018) The effect of some indoor ornamental plants on CO_2 levels during the day. Polish J Environ Stud 27:839–844. https://doi.org/10.15244/pjoes/76243

Shahane HA, Patel S (2021) Influence of curing method on characteristics of environment-friendly angular shaped cold bonded fly ash aggregates. J Build Eng. https://doi.org/10.1016/j.jobe.2020.101997

Shin HO, Yoo DY, Lee JH (2018) Development of 300 MPa ultra-high-strength mortar through a special curing regime. Constr Build Mater 171:312–320. https://doi.org/10.1016/j.conbuildmat.2018.03.134

Shubbar AA, Jafer H, Dulaimi A et al (2018) The development of a low carbon binder produced from the ternary blending of cement, ground granulated blast furnace slag and high calcium fly ash: An experimental and statistical approach. Constr Build Mater 187:1051–1060. https://doi.org/10.1016/j.conbuildmat.2018.08.021

Singh B, Ishwarya G, Gupta M, Bhattacharyya SK (2015) Geopolymer concrete: a review of some recent developments. Constr Build Mater 85:78–90. https://doi.org/10.1016/j.conbuildmat.2015.03.036

SinghSandhu G, Singh Salaria D (2014) A Bayesian network model of the particle swarm optimization for software effort estimation. Int J Comput Appl 96:52–58. https://doi.org/10.5120/16786-6371

Sobrosa FZ, Stochero NP, Marangon E, Tier MD (2017) Development of refractory ceramics from residual silica derived from rice husk ash. Ceram Int 43:7142–7146. https://doi.org/10.1016/j.ceramint.2017.02.147

Soltaninejad M, Soltaninejad M, Farshad Saberi K et al (2021) Environmental-friendly mortar produced with treated and untreated coal wastes as cement replacement materials. Clean Technol Environ Policy 23:2843–2860. https://doi.org/10.1007/s10098-021-02204-x

Subashi De Silva GHMJ, Vishvalingam S, Etampawala T (2021) Effect of waste rice husk ash from rice husk fuelled brick kilns on strength, durability and thermal performances of mortar. Constr Build Mater. https://doi.org/10.1016/j.conbuildmat.2020.121794

Suda VBR, Rao PS (2020) Experimental investigation on optimum usage of Micro silica and GGBS for the strength characteristics of concrete. In: Materials today: proceedings, pp 805–811

Suleiman AR, Nehdi ML (2017) Modeling self-healing of concrete using hybrid genetic algorithm-artificial neural network. Materials 10:135. https://doi.org/10.3390/ma10020135

Sun J, Wang J, Zhu Z et al (2022) Mechanical performance prediction for sustainable high-strength concrete using bio-inspired neural network. Buildings 12:65. https://doi.org/10.3390/buildings12010065

Taffese WZ, Sistonen E (2017) Machine learning for durability and service-life assessment of reinforced concrete structures: recent advances and future directions. Autom Constr 77:1–14

Tayeh BA, Hamada HM, Almeshal I, Bakar BHA (2022) Durability and mechanical properties of cement concrete comprising pozzolanic materials with alkali-activated binder: A comprehensive review. Case Stud Constr Mater 17:e01429. https://doi.org/10.1016/j.cscm.2022.e01429

Turkyilmaz A, Cetin M, Sevik H et al (2020) Variation of heavy metal accumulation in certain landscaping plants due to traffic density. Environ Dev Sustain 22:2385–2398. https://doi.org/10.1007/s10668-018-0296-7

Umasabor RI, Okovido JO (2018) Fire resistance evaluation of rice husk ash concrete. Heliyon 4:e01035. https://doi.org/10.1016/j.heliyon.2018.e01035

Varol T, Canturk U, Cetin M et al (2021) Impacts of climate change scenarios on European ash tree (*Fraxinus excelsior* L.) in Turkey. For Ecol Manag 491:119199. https://doi.org/10.1016/j.foreco.2021.119199

Varol T, Cetin M, Ozel HB et al (2022) the effects of climate change scenarios on *Carpinus betulus* and *Carpinus orientalis* in Europe. Water Air Soil Pollut. https://doi.org/10.1007/s11270-022-05516-w

Wang SD, Scrivener KL (1995) Hydration products of alkali activated slag cement. Cem Concr Res 25:561–571. https://doi.org/10.1016/0008-8846(95)00045-E

Yun CM, Rahman MR, Phing CYW et al (2020) The curing times effect on the strength of ground granulated blast furnace slag (GGBFS) mortar. Constr Build Mater. https://doi.org/10.1016/j.conbuildmat.2020.120622

Zhang Z, Liu S, Yang F et al (2021) Sustainable high strength, high ductility engineered cementitious composites (ECC) with substitution of cement by rice husk ash. J Clean Prod. https://doi.org/10.1016/j.jclepro.2021.128379